Collapse of genetic division of labour and evolution of autonomy in pellicle biofilms

Dragoš, Anna; Martin, Marivic; Garcia, Carolina Falcón; Kricks, Lara; Pausch, Patrick; Heimerl, Thomas; Bálint, Balázs; Maróti, Gergely; Bange, Gert; López, Daniel

Total number of authors:
12

Published in:
Nature Microbiology

Link to article, DOI:
10.1038/s41564-018-0263-y

Publication date:
2018

Document Version
Peer reviewed version

Collapse of genetic division of labour and evolution of autonomy in pellicle biofilms.

Anna Dragoš[1,2], Marivic Martin[1,2], Carolina Falcón Garcia[3], Lara Kricks[4], Patrick Pausch[5], Thomas Heimerl[6], Balázs Bálint[7,#], Gergely Maróti[8], Gert Bange[5], Daniel López[4], Oliver Lieleg[3], Ákos T. Kovács[1,2]

[1] Bacterial Interactions and Evolution Group, Department of Biotechnology and Biomedicine, Technical University of Denmark, 2800 Kgs Lyngby, Denmark

[2] Terrestrial Biofilms Group, Institute of Microbiology, Friedrich Schiller University Jena, 07743 Jena, Germany

[3] Department of Mechanical Engineering and Munich School of Bioengineering, Technical University of Munich, 85748 Garching, Germany

[4] National Centre for Biotechnology (CNB), Spanish Research Council (CSIC), 28049 Madrid, Spain.

[5] Faculty of Chemistry & LOEWE Center for Synthetic Microbiology, Philipps-University Marburg, 35043 Marburg, Germany

[6] Cell Biology & Electron Microscopy, LOEWE Center for Synthetic Microbiology, Philipps-University Marburg, 35043 Marburg, Germany

[7] Seqomics Biotechnology Ltd., 6782 Mórahalom, Hungary

[8] Institute of Plant Biology, Biological Research Centre, Hungarian Academy of Sciences, 6726 Szeged, Hungary

* Corresponding author: Bacterial Interactions and Evolution Group, Department of Biotechnology and Biomedicine, Technical University of Denmark, Søltofts Plads Building 221, 2800 Kgs Lyngby, Denmark; Tel: +45 45 252527; Fax: +45 45 932809 E-mail: atkovacs@dtu.dk

[#] Current address: Synthetic and Systems Biology Unit, Institute of Biochemistry, Biological Research Centre, Hungarian Academy of Sciences, 6726 Szeged, Hungary

ABSTRACT

Closely related microbes often cooperate, but the prevalence and stability of cooperation between different genotypes remains debatable. Here, we track the evolution of pellicle biofilms formed through genetic division of labour and ask whether partially deficient partners can evolve autonomy. Pellicles of *Bacillus subtilis* rely on an extracellular matrix composed of exopolysaccharide (EPS) and the fibre protein TasA. In monocultures, Δ*eps* and Δ*tasA* mutants fail to form pellicles, but, facilitated by cooperation, they succeed in co-culture. Interestingly, cooperation collapses on an evolutionary timescale, and Δ*tasA* gradually outcompetes its partner Δ*eps*. Pellicle formation can evolve independently from division of labour in Δ*eps* and Δ*tasA* monocultures, by selection acting on the residual matrix component, TasA or EPS respectively. Using a set of interdisciplinary tools, we unravel that the TasA-producer (Δ*eps*) evolves via an unconventional but reproducible substitution in TasA that modulates the biochemical properties of the protein. On the contrary, the EPS-producer (Δ*tasA*) undergoes genetically variable adaptations, all leading to enhanced EPS secretion and biofilms with different biomechanical properties. Finally, we revisit the collapse of division of labour between Δ*eps* and Δ*tasA* in light of a strong frequency vs. exploitability trade-off that manifested in the solitarily evolving partners. We propose such trade-off differences may represent an additional barrier to evolution of division of labour between genetically distinct microbes.

INTRODUCTION

Cooperation among microbes is indisputable, but the mechanism of partner selection remains under discussion. According to the fundamental theory of kin selection, cooperation should predominantly occur within closely related groups, where the chances that a beneficiary carries the same cooperative gene are maximized [1]. Nevertheless, it has been documented that individuals of low genetic relatedness can help each other, as long as they share a locus encoding for cooperation or a mechanism exists that allows discrimination against non-cooperators [2–5]. Cooperation may also take place via division of labour between (sub)populations of cells carrying/expressing different cooperative loci [6–8]. Benefits from allocation of cooperative tasks between different subpopulations or even genetically different strains have been demonstrated both experimentally [8–10] and by modelling [11,12]. Whereas, in phenotypic division of labour, task allocation is achieved by differences in gene expression, in the genetic one, individuals carry only the genetic machinery for their own specialist task [13].
Moreover, spontaneous deletions [14] potentially leading to cooperative metabolic exchange [15], and even spontaneous evolution of genetic division of labour [10], have been experimentally documented. Nevertheless, some models predict that cooperative trading between genetically 'reduced' partners is evolutionarily unstable due to risks of partner separation or social cheating [16,17].

Recent studies that directly tested the long-term stability of cooperation revealed that the evolutionary fate of social interactions can be unpredictable [18,19]. In the long-term presence of cheaters, cooperation may be reduced [20,21], or rewired towards another type of public good[20]. In particular cases, typically constrained defectors can spread as a side-effect of evolutionary awakening of mobile genetic elements [19]. Finally, co-operators can *de novo* evolve from defectors, sometimes exhibiting high resistance against exploitation [22], while being highly vulnerable to invasions by cheaters in other cases [23]. Altogether, social evolution is a very dynamic process where exploiters easily evolve [24]; their presence modulates the evolution of cooperators [20,21], which, even if extinct, may revive from defectors [22]. In the light of such complexity, without direct experimental examination, the long-term evolutionary fate of cooperation within or beyond single genetic lineages is difficult to predict.

Here, we experimentally challenged the long-term evolutionary stability of genetic division of labour and explored the solitary adaptation of partially defective partners. The study was performed using a simple model system where two *Bacillus subtilis* strains, when co-inoculated, benefit from division of labour in extracellular matrix construction by exchanging key matrix components: exopolysaccharide (EPS) and an amyloid protein, TasA [24]. These components form an extracellular matrix that allows *B. subtilis* to establish pellicle biofilms at the oxygen rich liquid-air interface [25]. Pellicles emerge when *B. subtilis* grows in undisturbed liquid medium and encounters oxygen limitation [25]. Mutants lacking

either EPS or TasA cannot establish pellicle biofilms, but they can complement each other in co-culture [19,30,31]. Previous studies suggest that such division of labour pays off and should be stable over evolutionary timescales [8]. Here, we directly challenge this hypothesis using an experimental evolution approach, hoping to reveal co-adaptation mechanisms of cooperating partners. Our work reveals an unexpected scenario regarding the fate of cooperation and striking adaptive trajectories followed by solitarily evolving partners.

RESULTS

Collapse of division of labour and evolution of autonomy in *B. subtilis* pellicles

Our initial goal was to study co-adaptation of partners Δ*eps* and Δ*tasA* involved in genetic division of labour, which seems an evolutionary stable and more productive strategy for biofilm formation compared to that employed by the isogenic wild-type (WT) bacteria [8]. In addition, the Δ*eps* and Δ*tasA* strains were allowed to adapt in monocultures (see methods).

In line with previous findings [8], the first pellicles formed by the mixtures showed very high productivity compared to the initial pellicles formed by solitarily grown Δ*eps* and Δ*tasA* (Fig. 1a–c, transfer 0; Fig. 1d). In addition, although inoculated at 1:1 ratio, the pellicles consisted of a Δ*eps* minority and a Δ*tasA* majority, a mixture which was previously identified as an evolutionarily stable optimum [8].
Surprisingly, the productivities in all the mixed cultures dropped by transfer 5 and remained low until transfer 24, rising again after transfer 29 or 35 (Fig. 1a). It was evident that the rapid decrease in pellicle productivities coincided with an increase in the frequency of Δ*tasA* cells in the co-cultures and the permanent domination of this strain thorough the experiment, even at the late evolutionary time points where productivities were rising again — indicating that after a depression, the mutant adapted to colonize the interface without the help of strain Δ*eps* (Fig. 1a–d). Ultimately, the Δ*eps* strain showed complete extinction in four out of six initially mixed parallel populations. An identical scenario was observed when experimental evolution was repeated from fresh culture stocks: a decrease in overall productivity and an increase in Δ*tasA* frequency (Supplementary Fig. 1a).

In monocultures, both mutants evolved mechanisms that allowed colonization of the liquid-air interface independently (Fig. 1b–d). Nevertheless the “success rate” of the adaptive process seemed to differ between the mutants since only two out of six parallel populations of Δ*eps* showed improvement, in contrast to increased air-medium colonization by all populations of Δ*tasA* (Fig. 1b–d). For both Δ*eps* and Δ*tasA* the final pellicles lacked the typical “wrinkled” surface complexity that can be

observed for the WT or the initial mix of mutants (Fig. 1d). However, a densely packed mat on the liquid surface could easily be observed on the macro-scale (Fig. 1d), as well as at the single-cell level (Supplementary Fig. 1b – see Methods). Specifically, cells of the evolved Δ*eps* seemed tightly packed, and the evolved Δ*tasA* pellicle appeared as a loosely connected mesh of cells and intracellular space (Supplementary Fig. 1b). Importantly, the phenotype and final productivities of evolved Δ*tasA* were nearly identical regardless of its evolutionary history (initiated in co-culture vs. in monoculture). Nevertheless, the evolution of independence by Δ*tasA* was delayed when it started in co-culture with Δ*eps* (Fig. 1a, c–d).

'Alter' strategy: EPS-independent pellicle formation involves modification of TasA protein

As a next step, we aimed to untangle the molecular mechanisms that allowed the Δ*eps* mutants to colonize the liquid-air interface. We selected three representative single clones from monoculture populations 4 and 6 (which we named e4A, e4B, e4C and e6A, e6B and e6C, respectively) that showed pellicle development, as well as two representatives of non-pellicle formers coming from population 3 (e3A) and population 5 (e5A), for whole genome sequencing. All adapted strains, but none of the non-pellicle forming negative controls, were found to contain single nucleotide polymorphisms (SNPs) in the *tasA* locus (Supplementary Dataset 1). Strikingly, these SNPs were distinct in population 4 and population 6, but they resulted in a substitution of an amino acid to cysteine in both cases, specifically Y124C in population 4 and G183C in population 6 (Supplementary Dataset 1).

Since TasA is a putative amyloid fibre protein [31–33], and cysteine plays important roles in protein oligomerization (reviewed in [33]), the introduction of this amino acid into TasA could have dramatic effects on its amyloidogenesis. Moreover, comparison of TasA proteins across different Firmicutes (the phylum to which *Bacillus* belongs) revealed a conservative lack of cysteines in this protein, while positions Y124 and G183 that were replaced by cysteines in the evolved Δ*eps* are located in the most conserved regions of TasA (Supplementary Fig. 2).

To test whether a single substitution in TasA can restore pellicle formation in the absence of EPS, we introduced $tasA_{Y124C}$ and $tasA_{G183C}$ into the ectopic *amyE* locus of the Δ*eps*Δ*tasA* double mutant, so that the original *tasA* was replaced by the cysteine-containing variants, resulting in Δ*eps*Δ*tasA*_$tasA_{Y124C}$ and Δ*eps*Δ*tasA*_$tasA_{G183C}$ strains (see Methods). Both substitutions completely restored the dense biofilm mat for strains Δ*eps*Δ*tasA*_$tasA_{Y124C}$ and Δ*eps*Δ*tasA*_$tasA_{G183C}$ in an isopropyl β-D-1-thiogalactopyranoside (IPTG)-dependent manner (Fig. 2a, Supplementary Fig. 3), but not in the control strain Δ*eps*Δ*tasA*_$tasA_{anc}$ where the native *tasA* was inserted into the *amyE* locus (Fig. 2a). This result

was supported by quantitative measurements of pellicle productivity, where the Δ*eps* ancestor (Δeps_{anc}) and Δ*eps*Δ*tasA_*$tasA_{anc}$ performed poorly, while the evolved (e4A, e6A) or complemented (Δ*eps*Δ*tasA_*$tasA_{Y124C}$, Δ*eps*Δ*tasA_*$tasA_{G183C}$) strains carrying cysteine-containing TasA showed tremendous and comparable improvement (Fig. 2b). Moreover, relative fitness of Δ*eps*Δ*tasA_*$tasA_{Y124C}$ and Δ*eps*Δ*tasA_*$tasA_{G183C}$ was higher than that of to Δeps_{anc} (Fig. 2c), whereas the Δ*eps*Δ*tasA_*$tasA_{anc}$ control strain did not show increased fitness when competed with Δeps_{anc} (Fig. 2c). Altogether, these results indicated that substitutions of certain residues in TasA to cysteine allow pellicle formation in the absence of EPS (Fig. 2c).

- **TasA evolves different biochemical properties and different amyloid fibre morphology**

How does the presence of cysteine change the properties of TasA? First, we asked whether it results in different biochemical properties of TasA that modulate oligomerization of the protein. To answer this question, we performed electrophoresis under native conditions combined with immunoblotting to detect TasA protein (see Methods). The native TasA (detected in Δeps_{anc} and Δ*eps*Δ*tasA_*$tasA_{anc}$) formed oligomers of ~900 kDa, while the oligomers formed by the evolved variants showed both a smaller band (~800kDa) and a smear at around 1000–1100 kDa (Supplementary Fig. 4b). It is highly unlikely that these results, or the results of complementation assays (Fig. 2), were affected by differences in the production levels of ancestral and evolved TasA variants, as SDS-PAGE combined with immunoblotting showed nearly identical band intensities for $TasA_{anc}$ (produced by Δeps_{anc} or Δ*eps*Δ*tasA_*$tasA_{anc}$) and for the cysteine-containing variants (produced by the evolved or complemented strains) (Supplementary Fig. 4a).

Does the difference in oligomerization manifest in amyloid fibre formation by TasA? To explore this, we purified and visualized the fibres using transmission electron microscopy (see methods, Supplementary Fig. 4c). All TasA variants showed formation of fibrous structures (Fig. 3) similar to those observed previously [31]. However, while native TasA showed a dense mesh of less organized, relatively thin fibres, the cysteine-containing variants assembled into thicker fibres that were formed by multiple, parallel arranged thin fibres (Fig. 3, Supplementary Fig. 4d). For $TasA_{anc}$, we observed bundles up to a fiber width of 20 nm. For the evolved TasA variants, we observed bundle widths up to 40 nm and 120 nm for $TasA_{Y124C}$ and $TasA_{G183C}$, respectively (Supplementary Fig. 4d). Based on the obtained electron micrographs, we speculate that the biochemical properties of the evolved, cysteine-containing TasA variant might be altered, which seems to influence filament architecture. However, more detailed studies are required to determine the exact structural properties of the evolved TasA protein and its filaments (e.g. by NMR and X-ray scattering) [34].

- **Cysteine-containing TasA likely interacts with other components of the extracellular matrix**

The above results suggested that cysteine-containing TasA can result in a dramatic fitness advantage (Fig. 2); therefore, the conserved absence of this amino acid from native TasA proteins present in Firmicutes seemed puzzling (Supplementary Fig. 2). To explore this contradiction, we examined the effects of Y124C and G183C substitutions in TasA in the WT *B. subtilis* background, where the EPS component is still present, $tasA_{anc}$, $tasA_{Y124C}$ and $tasA_{G183C}$ were introduced into the *amyE* locus of Δ*tasA* ancestor. Surprisingly, the presence of cysteine-containing TasA hindered biofilm productivity, hydrophobicity and surface spreading (Supplementary Fig. 5A-F, Supplementary Fig. 6, Supplementary Result 1).

Recently, it was shown that the main biofilm hydrophobin, BslA, carries a conserved CXXC motif on its C-terminal tail, which is crucial for protein oligomerization and therefore the hydrophobicity of *B. subtilis* biofilms [35]. Further experiments suggest that putative TasA-BslA interaction might interfere with proper biofilm maturation in the EPS-producing background (Supplementary Fig. 5d, Supplementary Results 2).

'Make more' strategy: TasA-independent pellicle formation involves overexpression of *epsA–O*

Whole genome sequencing of selected Δ*tasA* single isolates revealed multiple mutations that could potentially improve its fitness, but we could not identify one common locus that was changed in all isolates during improved surface colonization (Supplementary Dataset 1). Interestingly, despite strong genetic diversity, all the evolved surface-colonizers produced very similar, remarkably slimy pellicles (Fig. 1d, Supplementary Fig. 7a), which strongly differed in texture from mats of the WT or evolved Δ*eps* derivatives (see Fig. 1d for evolved Δ*eps* and Supplementary Fig. 5b for WT pellicle structures). Indeed, the rheology studies performed on selected evolved Δ*tasA* isolates (Mt1a evolved from coculture mix 1 and t5A-isolated from monoculture population 5), WT and evolved Δ*eps* revealed that the elastic moduli obtained for the WT and evolved Δ*eps* isolates (e4A, e6A) were 2–3 log higher than those obtained for the evolved Δ*tasA* strains, indicating low stiffness of the latter. In addition, the higher loss factor values obtained for the evolved Δ*tasA* compared to the WT and evolved Δ*eps* isolates indicated increased viscosity of the evolved Δ*tasA* pellicles (Fig. 4a, Supplementary Fig. 7b).

Slimy surfaces of bacterial colonies, similar to that observed for the evolved Δ*tasA* pellicles, might be associated with increased production of the exopolysaccharide [36]. To test this possibility , we compared the amounts of EPS produced per dry biomass in WT, ancestral Δ*tasA*, Δ*tasA* overexpressing *epsA–O* from an IPTG-inducible $P_{hyperspank}$ promoter ($\Delta tasA_{hyEPS}$), Δ*eps* (used as a negative control), and selected

evolved strains (see Methods, Supplementary Fig. 7c). The results pointed towards increased production of EPS by the evolved strains (Supplementary Fig. 7c). In the next step, a P_{eps}-*gfp* promoter fusion was introduced into randomly selected evolved Δ*tasA* isolates and their *epsA–O* expression levels were compared with the ancestor Δ*tasA* under planktonic conditions in the biofilm-promoting MSgg medium. All examined evolved strains showed a higher GFP signal than $\Delta tasA_{anc}$ (Fig. 4b). The same result was evident from assaying *epsA–O* expression in biofilm colonies (with one exception, strain t6B, which also showed the lowest GFP signal among the evolved Δ*tasA* strains in the quantitative assay) (Supplementary Fig. 8a). We presume that one of the possible SNPs resulting in overproduction of EPS could be a mutation in the *ptpZ* gene (Supplementary Table 1, Fig. 4c-d, Supplementary Fig. 8b, Supplementary Results 3). Finally, we examined pellicle formation of $\Delta tasA_{hyEPS}$ in both the presence and absence of IPTG. As expected, in the presence of IPTG, $\Delta tasA_{hyEPS}$ produced a comparable slimy pellicle phenotype, with identical biophysical properties and pellicle productivity, to the evolved Δ*tasA* strains (Fig. 4c–d, Supplementary Fig. 7b).

This result confirmed that in analogy to Δ*eps,* the adaptation of Δ*tasA* involved the remaining matrix component, EPS. However, here, the improvement could simply be achieved through overproduction. Interestingly, some of the evolved Δ*eps* isolates also showed increased *tasA* expression (Supplementary Fig. 8c), but simple overexpression of ancestor *tasA* (using strain Δ*eps*ΔtasA_$tasA_{anc}$ at high IPTG concentrations) did not translate into improved pellicle formation (Fig. 2b).

The adaptive strategy of the EPS- and TasA-producer is associated with low and high exploitability levels, respectively

Next, we asked what the implications of the two adaptive strategies ('alter' for Δ*eps* and 'make more' for Δ*tasA*) were on population dynamics of the evolved lineages and on subsequent changes in relative fitness during evolution (see methods).

The structures of the evolved Δ*eps* populations exhibited an 'all or nothing' pattern, where either all isolates within the population behaved like the ancestor, or nearly all of them showed robust pellicle development (Fig. 5a). On the contrary, all examined populations of Δ*tasA* exhibited high diversity with respect to ability to form pellicles (Fig. 5c). The results of this large-scale, but purely qualitative, screen were supported by smaller-scale quantitative assays that confirmed low and high phenotypic diversity within the evolved Δ*eps* and evolved Δ*tasA* populations respectively (Supplementary Fig. 9). Relative fitness analysis highlighted further differences between the adaptive patterns of Δ*eps* and Δ*tasA* populations. Namely, populations of Δ*eps* from subsequent evolutionary time points showed, in general terms, a steady increase in relative fitness compared with the ancestor (Fig. 5b, Supplementary

Fig. 10a). In contrast, while populations of Δ*tasA* from early evolutionary time-points showed an increase in relative fitness, the advantage diminished in later populations, as the ancestor was able to hitchhike with the improved pellicle-formers, possibly exploiting the EPS secreted by the evolved population (Fig. 5d, Supplementary Fig. 10b). These results point towards exploitability differences between the evolved Δ*eps* and Δ*tasA* strains: while hitchhiking of poorly-performing isolates within the evolved Δ*eps* populations is limited, it seems prevalent in the case of the evolved Δ*tasA* populations.

Disparity in the adaptive potential of cooperating partners may predestine the cooperation to collapse

As both strains Δ*eps* and Δ*tasA* could adapt in monocultures, delivering pellicles of comparable productivities, we further wondered why cooperation between the Δ*eps* and Δ*tasA* mutant strains collapsed. Specifically, we were interested in the link between the frequency increase of Δ*tasA* and the overall productivity loss that consistently happened at the beginning of coevolution (Fig. 1a). Therefore, the productivity of the Δ*eps* and Δ*tasA* mix was assessed in three alternative scenarios: a) Δ*tasA* adapts before Δ*eps;* b) Δ*eps* adapts before Δ*tasA;* c) both strains adapt at the same time. To artificially simulate such scenarios, the productivities of mixed pellicles formed by (a) Δeps_{anc} + evolved Δ*tasA*, (b) evolved Δ*eps* + $\Delta tasA_{anc}$, and (c) evolved Δ*eps* + evolved Δ*tasA* were compared to the productivity of the ancestral mix. Nearly all Δeps_{anc} + evolved Δ*tasA* mixes developed pellicles with lower productivity compared to the ancestral mix, while evolved Δ*eps* + $\Delta tasA_{anc}$ mixes tended to perform better than or similar to the ancestors (Fig. 6). Therefore, the performance of the mix was negatively affected when Δ*tasA*, but not Δ*eps,* was preadapted to pellicle growth conditions*,* but improved with the opposite combination (Fig. 6). In addition, the absence of Cys-containing TasA variant in the Δeps_{evo} had negative effect on its relative frequency in co-culture with $\Delta tasA_{evo,}$ (Supplementary Fig. 10d).

As previous results suggest that EPS is exploitable [8] and that evolved Δ*tasA* strains serve as EPS-overproducers, we directly assessed how EPS overproduction by Δ*tasA* (in the absence of other adaptive mutations) would influence growth dynamics in pellicles. Interestingly, overproduction of EPS by Δ*tasA* had positive effects on the total productivity, and it improved the productivity of the Δ*eps* strain in the mix. This suggests that the cooperation collapse was due to other mutations occurring in the evolved Δ*tasA* (Supplementary Fig. 10c). To test whether, during early stages of coevolution, the Δ*tasA* was able to accumulate/fix more SNPs than Δ*eps*, the populations of Δ*eps* and Δ*tasA* obtained from transfers 5, 15 and 25 were subjected to resequencing. Unexpectedly, nearly all mutations

previously identified for coevolved Δ*eps* and Δ*tasA* were already present in all populations from transfer 5 at nearly 90% frequency (Supplementary Dataset 1).

Finally, we assessed whether, in contrast to the ancestor, the evolved Δ*eps* and Δ*tasA* can coexist on an evolutionary time scale. Interestingly, several of evolved Δ*tasA* + evolved Δ*eps* collocations showed higher pellicle productivities than the ancestral mix (Fig. 6) and in general the frequencies were shifted towards Δ*eps* abundance compared to the ancestral mix (Supplementary Fig. 10d). Indeed, we have also observed that preadaptation of Δ*eps* and Δ*tasA* to independent surface colonization facilitated their long-term coexistence (Supplementary Fig. 11).

The above results indicate that the evolutionary advantage of Δ*tasA* results in diminishing frequencies of Δ*eps* in the mix, preventing its adaptation and leading to collapse of the division of labour. Such a scenario, although suboptimal for both partners, is likely to occur (Supplementary Fig. 11).

DISCUSSION

Prevalence of cooperation beyond isogenic populations of microbes remains controversial. Here, using an experimental evolution approach, we challenged the long-term stability of genetic division of labour during pellicle biofilm formation. Although both partially defective strains gained significant net benefits from coexistence, pervasive dominance of one partner (Δ*tasA*) repeatedly triggered the collapse of cooperation. Specifically, the overabundance of an EPS-producer (Δ*tasA*) and the diminished frequency of a TasA-producer (Δ*eps*) led to an imbalance in extracellular matrix composition and therefore low pellicle productivity, resulting in populations mimicking the composition of solitary Δ*tasA* lineages. Interestingly, the productivities of the Δ*tasA* lineages from the originally mixed populations were delayed compared to monoculture-initiated populations that lacked the cooperation-collapse history. Therefore, in addition to being unstable, cooperation also inferred long-term negative consequences for both members of the original population, leading to extinction of Δ*eps* and slowing down the adaptation of Δ*tasA*.

Recently, spontaneous emergence of ´genetic division of labour´ was observed during adaptive radiation of *Pseudomonas aeruginosa* [10]. As the evolved variants differed only in levels of the biofilm messenger cyclic di-GMP, they could undergo reciprocal reversions, potentially rescuing cooperation from a collapse caused by the dominance of the more abundant partner. On the contrary, in our approach division of labour was highly sensitive to disturbances in the relative frequencies of the two partners. Strikingly, experimental [10,14] and computational[11] studies suggest that mutually beneficial interactions can frequently evolve and provide fitness benefits to the whole population [9,10]. However,

not all mutually beneficial behaviours account for cooperation [39], which as such may rarely be maintained beyond genetic lineages[16,40,41].

Our work indicates that when defectors take over the population, alternative survival strategies might evolve, demonstrating that cooperation collapse does not lead to evolutionary dead-end and population extinction. While newly evolved mechanisms of pellicle formation were based on the remaining matrix components, TasA or EPS respectively, they differed in frequency of occurrence, strategy and vulnerability to exploitation.

The EPS-producing Δ*tasA* evolved through a more 'feasible' strategy, which we termed 'make more', as it simply involved overproduction of EPS. Similar adaptive strategies were previously observed in several unrelated species, including *P. fluorescens* or *P. aeruginosa* that evolved to overproduce cellulose[42] or alginate[36], respectively. Matrix overproduction not only allows niche expansion [10,42,36], but also helps to cope with stress caused by predators[43] or the immune system of a host[44]. As secreted exopolysaccharides are products of several enzymes controlled by numerous regulators, many genes serve as potential targets for acquisition of mutation(s) that could lead to increased EPS synthesis. Nevertheless, previous studies and our work [23,24,45] point towards the vulnerability of such a strategy to social exploitation, indicating that it may represent a feasible but possibly also unstable evolutionary solution.

Our results also reveal anotheradaptive pattern in the absence of EPS, based on a single amino acid substitution in the protein matrix component, TasA. In contrast to the 'make more' strategy observed in the case of the EPS-producer, the TasA-producer employed the so called 'alter' approach, which, although less likely to occur, is evolutionarily more stable. Molecular studies revealed interesting properties of cysteine-containing TasA: an altered oligomerization pattern that might translate into assembly of initially smaller fibres into strengthened parallel fibres that provide a robust chassis for cells lacking EPS. However, these larger fibres might generate a porous biofilm, as revealed by wetting studies using WT strains carrying $TasA_{Y124C}$ or $TasA_{G183C}$ in the presence of EPS. Alternatively, loss of non-wetting behaviour could be explained by interactions with BslA (especially in the case of the $TasA_{Y124C}$ derivative). Lack of a positive effect on fitness combined with biofilm porosity likely explains the persistent lack of cysteines in TasA proteins of other Bacilli. Cysteine-containing TasA might exist in EPS-deficient strains, but such may be vastly undersampled due to atypical colony morphology [24,25,31].

Importantly, in addition to matrix-related mutations, other adaptive mutations could contribute to productivity of the evolved strains. For instance, numerous mutations were detected that could modify motility (*fliY, fliG*) in some of the evolved Δ*eps* strains, and anaerobic respiration (*rex*), chemotaxis (*mcpC* and *cheA*) or aerotaxis (*hemAT*) in the evolved Δ*tasA* strains (Supplementary Dataset 1).

There are important questions remaining as to the underlying evolutionary dynamics in Δ*eps*+Δ*tasA* co-culture system. Still, evolutionary success of the solitarily grown defectors allowed deeper understanding of their failure as a cooperative community. Specifically, early evolutionary events resulted in dominance of Δ*tasA* in co-cultures, quickly reducing the prevalence of Δ*eps*, minimizing the feasibility of substitutions in TasA. Paradoxically, if Δ*eps* was evolutionarily ahead of Δ*tasA*, or both partners evolved in concordance, the community productivity might be superior. This is potentially caused by the higher exploitability of EPS compared to TasA [8]; therefore, a lower frequency of the EPS-producer could still offer sufficient quantities of this matrix component for the whole population (especially in the case of evolved strains that overproduce EPS).

While cooperation between different strains/lineages might be common during adaptive diversification or co-evolution of different strains or species, our work reveals possible vulnerabilities of this phenomenon and alternative, cooperation-independent solutions.

Methods

Strains and cultivation conditions. Supplementary Table S1 describes the strains used in this study and Supplementary Table S2 lists all strains from which gDNA was obtained to construct the strains needed. Plasmids and oligonucleotides used for cloning purposes to construct some of the strains used here are listed in Supplementary Table S3 and Supplementary Table S4, respectively. Strains were maintained in lysogeny broth (LB) medium (LB-Lennox, Carl Roth; 10 g/l tryptone, 5 g/l yeast extract, and 5 g/l NaCl), while MSgg medium was used for pellicle biofilm induction [25].

Experimental evolution and productivity assays

All strains used in this study originated from naturally competent derivatives of the undomesticated *B. subtilis* NCBI 3610 DK1042 strain [46]. Pellicles of *B. subtilis* can be constructed through interaction of two partially deficient mutants, Δ*eps* and Δ*tasA*, that exchange matrix components with each other [8,19,31]. The 1:1 initial ratio of Δ*eps* + Δ*tasA* mixtureswas adjusted based on OD_{600} values of corresponding overnight cultures. Pellicles (or residual pellicles in the case of Δ*eps* and Δ*tasA* monocultures) were grown in MSgg medium statically in a 24-well plate at 30°C for 48 h in six parallel replicates.

Experimental evolution was performed as previously described [24]. Specifically, six parallel co-cultures of Δ*eps* and Δ*tasA* mixed in an initial ratio of 1:1 were subjected to experimental evolution for 35 transfers, representing approximately 250 generations. Pellicles were monitored qualitatively at every transfer and relative frequencies of the mutants and pellicle productivities (i.e. CFU/ml) were quantified every five transfers. Mature pellicles were gently harvested from the surface of the MSgg medium using a plastic inoculating loop, transferred to 2-ml Eppendorf tubes containing 1 ml of 0.9% NaCl and 100 µl of glass sand, and vigorously vortexed for 1 min. This approach allowed effective disruption of the material into single cells and small clumps without a requirement for sonication (which would increase the risk of contamination). Finally, the populations were reinoculated after 100× dilution. In the case of the monoculture mutants, the thin layer of cells colonizing the liquid-air interface was carefully harvested, mildly disrupted and reinoculated using a proportionally lower dilution factor, to avoid strong bottleneck effects. After the 5th, 10th, 14th,19th, 24th, 29th and 35th pellicle transfers, Δ*eps* and Δ*tasA* frequencies (in the case of mixed pellicles) and colony forming units (CFU)/ml, described here as pellicle productivity, were monitored, and deep frozen (−80°C) stocks were preserved. Before each CFU assay, pellicles were sonicated according to a protocol optimized in our laboratory [19].

Population structure and relative fitness assay

To examine population structure in the evolved Δ*eps* and Δ*tasA* populations four final populations (from transfer 35) of solitarily evolved Δ*eps* and Δ*tasA* were selected and 96 randomly picked isolates per population were screened for performance. The ability of the isolates to make pellicles was qualitatively evaluated and scored from 0 (performs like the ancestor, no pellicle) to 3 (forms a strong pellicle).

For relative fitness assay: strains/populations of interest were premixed at a 1:1 ratio based on their OD_{600} values and the mixture was inoculated into MSgg medium at 1%. The ancestral strains (Δ*eps* or Δ*tasA*) that were used for the fitness assays carried an *amyE*::P_{ctc}-*lacZ* fusion allowing easy assessment of their relative frequencies on LB-agar plates containing X-Gal (5-bromo-4-chloro-3-indolyl β-D-galactopyranoside) substrate (40 µg/ml). Ancestral strains and populations from different evolutionary time points were allowed to compete for 48 h at 30°C in standard pellicle growth conditions. After that time, the pellicles were carefully harvested from the liquid surface, mildly sonicated and subjected to CFU assay. For relative fitness assays performed for ΔΔ*tasA*$_{anc}$, ΔΔ*tasA*$_{Y124C}$ and ΔΔ*tasA*$_{G183C}$, the MSgg medium was supplemented with 0.2 mM IPTG. Relative fitness W_A for strain A in competition with strain B was calculated as:

$W_A = [\ln(CFU_{A\_16h}/CFU_{A\_start})]/[\ln(CFU_{B\_16h}/CFU_{B\_start})]$

Western blotting

Strains were grown in MSgg medium and *tasA* was induced with 0.2 mM IPTG. Cultures were incubated in 24-well plates for 48 h at 30°C. To induce expression of *tasA*, MSgg medium was supplemented with 0.2 mM IPTG. Biofilms were dispersed by sonication for two pulses of 10 s each. Total protein amount was determined with Bradford reagent (Bio-Rad) and samples were normalized. Samples were resolved on 12% SDS-PAGE and proteins were transferred to a polyvinylidene fluoride (PVDF) membrane using wet blotting. Non-specific binding sites were blocked with 10% skimmed milk in TBST (Tris-buffered saline, 0.1% Tween 20) for 1 h at room temperature, followed by incubation with TasA antibody overnight at 4°C (antibody was kindly provided by Kürsad Turgay, Leibniz Universität Hannover) diluted 1:10,000 in TBST. The membrane was washed three times with TBST for 10 min each before and after incubation with the secondary antibody goat anti-rabbit IgG (diluted 1:20,000 in TBST; Bio-Rad) for 1 h at room temperature. Signal was developed with Clarity™ Western ECL Substrate (Bio-Rad) and detected with the Chemi Doc™ Touch Imaging System (Bio-Rad).

Blue-native PAGE

Preparation of cell lysates was performed as stated above. Normalized protein samples were loaded on a 3–12% Bis-Tris Gel (Invitrogen). Electrophoresis was performed according to manufacturer's instructions and proteins were transferred to PVDF membrane. The membrane was incubated for 15 min in 8% acetic acid, rinsed with water, air dried, and incubated in methanol for 1 min. The membrane was rinsed with water and a picture of the membrane was taken to record protein standard positions. Detection of TasA was performed as described above.

Expression and purification of TasA

His-tagged WT TasA, $TasA_{Y124C}$ and $TasA_{G183C}$, lacking the N-terminal signal peptide (ΔSP), were heterologously overexpressed in *Escherichia coli* and successfully purified by Ni-NTA affinity chromatography (Supplementary Fig. 4c) to visualize the corresponding amyloid fibres using transmission electron microscopy. Cloning of TasA is described in Table S3. Transformed *E. coli* BL21 (DE3) cells (Novagen) were inoculated into 100 ml LB medium supplemented with lactose (12.5 g/l) and kanamycin (50 mg/l). Cells were incubated at 30°C overnight with vigorous shaking (180 rpm). Cells were harvested by centrifugation (3,500 × *g*, 20 min, 4°C) and resuspended in 30 ml buffer A (20 mM HEPES-Na, pH 8.0, 250 mM NaCl, 20 mM KCl, 20 mM $MgCl_2$, 40 mM imidazole) before lysis in a M-110L Microfluidizer (Microfluidics). The lysate was cleared at 47,850 × *g* for 20 min at 4°C and the supernatant was transferred to a 50-ml Falcon tube; 300 µl washed Ni-NTA bead slurry (Ni-Sepharose 6 Fast Flow; GE) was added and incubated on ice for 20 min on a shaking platform at 50 rpm. Ni-NTA beads with bound TasA and TasA polymers were subsequently separated from the soluble fraction by

centrifugation at 3,200 × *g* for 5 min at 4°C, transferred into a 1.5-ml tube, and washed three-times with 1 ml buffer A. Proteins were eluted in 500 µl buffer B (20 mM HEPES-Na, pH 8.0, 250 mM NaCl, 20 mM KCl, 20 mM $MgCl_2$, 500 mM imidazole) and dialyzed overnight at 4°C into buffer C (20 mM Tris-Na, pH 7.4, 100 mM NaCl). Protein concentrations were determined as 1 µM for $TasA_{anc}$ and $TasA_{Y124C}$ and 0.5 µM for $TasA_{G183C.}$, by measuring the absorption at 280nm using a NanoDrop Lite Spectrophotometer. For visual and quantitative analysis of TEM micrographs, the regions in which TasA filaments and bundles were located and where the staining and carbon coating was of good quality, were selected.

Transmission electron microscopy analysis

Carbon coated copper grids (400 mesh) were hydrophilized by glow discharge (PELCO easiGlow, Ted Pella, USA). Protein suspensions (5 µl) with concentration 0.5 or 1 µM were applied onto the hydrophilized grids and stained with 2% uranyl acetate after a short washing step with double-distilled H_2O. Samples were analysed with a JEOL JEM-2100 transmission electron microscope using an acceleration voltage of 120 kV. For image acquisition, a F214 FastScan CCD camera (TVIPS, Gauting) was used.

Rheological characterization

Rheological measurements were performed using a commercial shear rheometer (MCR 302; Anton Paar GmbH, Graz, Austria). To produce enough biofilm material, pellicles were grown in Petri dishes of 60 mm diameter for 48 h at 30°C and three mature pellicles were pooled to produce a single biological replicate. Frequency spectra from 0.1 to 10 Hz were obtained at 21°C using plate-plate geometry (PP25 measuring head, Anton Paar) and a measuring gap of 250–400 µm (depending on the amount of material obtained from pooling pellicles). Small torques (~1 µN·m) were applied to guarantee a linear material response. A pairwise significance analysis was performed. The p-values obtained are given in Table S5.

EPS precipitation

Strains were cultivated in MSgg medium at 30°C for 48 h with shaking at 225 rpm. Biomass was separated from the supernatant by centrifugation (10 min, 12000 × g). Biomass was dried (48 h at 55°C) and weighed. Supernatants were mixed with three volumes of cold 96% ethanol and precipitated for 24 h at 4°C. The precipitate was collected by centrifugation (10 min, 7500 × g) and resuspended in 0.4% NaCl solution (0.1 of initial supernatant volume). The suspension was again mixed with three volumes of cold 96% ethanol and allowed to precipitate for 24 h at 4°C. After this second precipitation

round, in all samples but Δ*eps*, the EPS could be observed as a white gel floating at the ethanol/air interface [47]. The gel was carefully collected using a syringe, transferred to a fresh Eppendorf tube and pelleted down (1 min, 12000 × g). The pellet was dried (48 h at 55°C) and weighed. Dry EPS mass was normalized to total dry biomass.

Microscopy/confocal laser scanning microscopy (CLSM)

Bright field and fluorescence images of whole pellicles and colonies were obtained with an Axio Zoom V16 stereomicroscope (Carl Zeiss, Germany) equipped with a 0.5× PlanApo Objective, two LED cold-light sources (one for fluorescence detection and one for the visible light), a HE 38 filter set for GFP (excitation at 470/40 nm and emission at 525/50 nm), a 63 HE filter set for RFP (excitation at 572/25 nm and emission at 629/62 nm), and an AxioCam MRm monochrome camera (Carl Zeiss). The pellicles were also analysed using a confocal laser scanning microscope (LSM 780 equipped with an argon laser, Carl Zeiss) and a Plan-Apochromat/1.4 Oil DIC M27 63× objective. Fluorescent reporter excitation was performed at 488 nm for green fluorescence and at 564 nm for red fluorescence, while the emitted fluorescence was recorded at 484–536 nm and 567–654 nm for GFP and mKate, respectively. To generate pellicle images, Z-stack series with 1 µm steps were acquired. Zen 2012 Software (Carl Zeiss) was used for both stereomicroscopy and CLSM image visualization.

Genome resequencing and genome analysis

Genomic DNA of selected isolated strains was extracted using the EURex Bacterial and Yeast Genomic DNA Kit from cultures grown for 16 h. Paired-end fragment reads (2 × 150 nucleotides) were generated using an Illumina NextSeq sequencer. Primary data analysis (base-calling) was carried out with "bcl2fastq" software (v.2.17.1.14, Illumina). All further analysis steps were done in CLC Genomics Workbench Tool 9.5.1. Reads were quality-trimmed using an error probability of 0.05 (Q13) as the threshold. In addition, the first ten bases of each read were removed. Reads that displayed ≥80% similarity to the reference over ≥80% of their read lengths were used in mapping. Non-specific reads were randomly placed to one of their possible genomic locations. Quality-based SNP and small In/Del variant calling was carried out requiring ≥8× read coverage with ≥25% variant frequency. Only variants supported by good quality bases (Q ≥ 20) were considered, and only when they were supported by evidence from both DNA strands. The genome of the wild-type ancestor was also re-sequenced to subtract the mutations that could have been present before the evolution experiment. Data on average coverage for each strain sequenced in this study is provided in Supplementary Table S5.

Statistical analyses

Statistical differences between two experimental groups were identified using two-tailed Student's *t*-tests assuming equal variance. Variances in the two main types of datasets (CFU counts in competition assays and weight of biomass) were similar across different samples and their normal distribution was confirmed using Kolmogorov–Smirnov ($P > 0.05$). No data points were removed from the dataset prior analyses. No statistical methods were used to predetermine sample size and the experiments were not randomized.

Data availability

All datasets generated and analysed during this study are available from corresponding author on request.

Acknowledgements

We thank S. West for his comments on our manuscript. This work was funded by the Deutsche Forschungsgemeinschaft (DFG) to Á.T.K. (KO4741/2.1) within the Priority Program SPP1617. A.D. and C.F.G. were supported by fellowships from the Alexander von Humboldt Foundation and Consejo Nacional de Ciencia y Tecnología (CONACyT), respectively. The research leading to these results has received funding from the European Union's Horizon 2020 research and innovation programme under the Marie Sklodowska-Curie grant agreement no. 713683 (COFUNDfellowsDTU). This work was also supported by the DFG through project B11 in the framework of SFB863 granted to O.L., and a start-up grant from the Technical University of Denmark to Á.T.K.

Authors contributions

A.D. and Á.T.K. conceived the project, A.D., M.M., C.F.G., L.K., P.P., and T.H. performed the experiments, B.B. performed NGS data analysis, G.M., G.B., D.L., and O.L. contributed with methods, analysed data and supervized experiments. A.D. and Á.T.K. wrote the manuscript, with all authors contributing to the final version.

Competing interests

The authors declare no competing interests.

Additional information

Supplementary information is available for this paper at https://doi.org/10.1038/ s41564-018-0263-y.

REFERENCES

1. Hamilton, W. D. The genetical evolution of social behaviour. I. *J. Theor. Biol.* **7,** 1–16 (1964).
2. Queller, D. C., Ponte, E., Bozzaro, S. & Strassmann, J. E. Single-gene greenbeard effects in the social amoeba *Dictyostelium discoideum*. *Science* **299,** 105–106 (2003).
3. Gibbs, K. A. & Greenberg, E. P. Territoriality in *Proteus*: advertisement and aggression. *Chem. Rev.* **111,** 188–94 (2011).
4. Kiers, T. E., Rousseau, R. A., West, S. A. & Denison R. Ford. Host sanctions and the legume-rhizobium mutualism. *Nature* **425,** 78–81 (2003).
5. West, S. A., Griffin, A. S. & Gardner, A. Review evolutionary explanations for cooperation. *Curr. Biol.* **17,** 661–672
6. Zhang, Z., Claessen, D. & Rozen, D. E. Understanding microbial divisions of labor. *Front. Microbiol.* **7,** 2070 (2016).
7. van Gestel, J., Vlamakis, H. & Kolter, R. From cell differentiation to cell collectives: *Bacillus subtilis* uses division of labor to migrate. *PLoS Biol.* **13,** e1002141 (2015).
8. Dragoš, A. *et al.* Division of labor during biofilm matrix production. *Curr. Biol.* **28,** 1903–1913 (2018).
9. Pande, S. & Kost, C. Bacterial unculturability and the formation of intercellular metabolic networks. *Trends Microbiol.* **25,** 349–361 (2017).
10. Kim, W., Levy, S. B. & Foster, K. R. Rapid radiation in bacteria leads to a division of labour. *Nat. Commun.* **7,** 10508 (2016).
11. Germerodt, S. *et al.* Pervasive selection for cooperative cross-feeding in bacterial communities. *PLOS Comput. Biol.* **12,** e1004986 (2016).
12. Lowery, N. V., McNally, L., Ratcliff, W. C. & Brown, S. P. Division of labor, bet hedging, and the evolution of mixed biofilm investment strategies. *MBio* **8,** e00672-17 (2017).
13. Wahl, L. M. The Division of Labor: Genotypic versus phenotypic specialization. *Am. Nat.* **160,** 135–145 (2002).
14. D'Souza, G. & Kost, C. Experimental evolution of metabolic dependency in bacteria. *PLoS Genet.* **12,** e1006364 (2016).
15. Morris, J. J., Lenski, R. E. & Zinser, E. R. The Black Queen Hypothesis: evolution of dependencies through adaptive gene loss. *MBio* **3,** e00036-12 (2012).
16. Oliveira, N. M., Niehus, R. & Foster, K. R. Evolutionary limits to cooperation in microbial communities. *Proc. Natl. Acad. Sci. U. S. A.* **111,** 17941–17946 (2014).
17. Cooper, G. A. & West, S. A. Division of labour and the evolution of extreme specialization. *Nat. Ecol. Evol.* **2,** 1161-1167 (2018).

18. Waite, A. J. & Shou, W. Adaptation to a new environment allows cooperators to purge cheaters stochastically. *Proc. Natl. Acad. Sci. U. S. A.* **109,** 19079–19086 (2012).
19. Martin, M. *et al. De novo* evolved interference competition promotes the spread of biofilm defectors. *Nat. Commun.* **8,** 15127 (2017).
20. O'Brien, S., Luján, A. M., Paterson, S., Cant, M. A. & Buckling, A. Adaptation to public goods cheats in *Pseudomonas aeruginosa*. *Proceedings. Biol. Sci.* **284,** (2017).
21. Kümmerli, R. *et al.* Co-evolutionary dynamics between public good producers and cheats in the bacterium *Pseudomonas aeruginosa*. *J. Evol. Biol.* **28,** 2264–2274 (2015).
22. Fiegna, F., Yu, Y.-T. N., Kadam, S. V. & Velicer, G. J. Evolution of an obligate social cheater to a superior cooperator. *Nature* **441,** 310–314 (2006).
23. Hammerschmidt, K., Rose, C. J., Kerr, B. & Rainey, P. B. Life cycles, fitness decoupling and the evolution of multicellularity. *Nature* **515,** 75–79 (2014).
24. Dragoš, A. *et al.* Evolution of exploitative interactions during diversification in *Bacillus subtilis* biofilms. *FEMS Microbiol. Ecol.* **94,** fix155 (2018).
25. Branda, S. S., Gonzalez-Pastor, J. E., Ben-Yehuda, S., Losick, R. & Kolter, R. Fruiting body formation by *Bacillus subtilis. Proc. Natl. Acad. Sci. U. S. A.* **98,** 11621–11626 (2001).
26. Chai, Y., Chu, F., Kolter, R. & Losick, R. Bistability and biofilm formation in *Bacillus subtilis. Mol. Microbiol.* **67,** 254–263 (2007).
27. Kobayashi, K. SlrR/SlrA controls the initiation of biofilm formation in *Bacillus subtilis*. *Mol. Microbiol.* **69,** 1399–1410 (2008).
28. Cozy, L. M. *et al.* SlrA/SinR/SlrR inhibits motility gene expression upstream of a hypersensitive and hysteretic switch at the level of σ^D in *Bacillus subtilis*. *Mol. Microbiol.* **83,** 1210–1228 (2012).
29. Kearns, D. B. You get what you select for: better swarming through more flagella. *Trends Microbiol.* **21,** 508–509 (2013).
30. Branda, S. S., Chu, F., Kearns, D. B., Losick, R. & Kolter, R. A major protein component of the *Bacillus subtilis* biofilm matrix. *Mol. Microbiol.* **59,** 1229–1238 (2006).
31. Romero, D., Vlamakis, H., Losick, R. & Kolter, R. An accessory protein required for anchoring and assembly of amyloid fibres in *B. subtilis* biofilms. *Mol. Microbiol.* **80,** 1155–1168 (2011).
32. Romero, D., Aguilar, C., Losick, R. & Kolter, R. Amyloid fibers provide structural integrity to *Bacillus subtilis* biofilms. *Proc. Natl. Acad. Sci. U. S. A.* **107,** 2230–2234 (2010).
33. Dragoš, A., Kovács, Á. T. & Claessen, D. The role of functional amyloids in multicellular growth and development of Gram-positive bacteria. *Biomolecules* **7,** 60 (2017).
34. Diehl, A. *et al.* Structural changes of TasA in biofilm formation of *Bacillus subtilis*. *Proc. Natl. Acad. Sci. U. S. A.* **115,** 3237–3242 (2018).

35. Arnaouteli, S. *et al.* Bifunctionality of a biofilm matrix protein controlled by redox state. *Proc. Natl. Acad. Sci. U. S. A.* **114,** E6184–E6191 (2017).
36. Kim, W., Racimo, F., Schluter, J., Levy, S. B. & Foster, K. R. Importance of positioning for microbial evolution. *Proc. Natl. Acad. Sci.* **111,** E1639–E1647 (2014).
37. Gao, T., Greenwich, J., Li, Y., Wang, Q. & Chai, Y. The bacterial tyrosine kinase activator TkmA contributes to biofilm formation largely independently of the cognate kinase PtkA in *Bacillus subtilis*. *J. Bacteriol.* **197,** 3421–3432 (2015).
38. Kiley, T. B. & Stanley-Wall, N. R. Post-translational control of *Bacillus subtilis* biofilm formation mediated by tyrosine phosphorylation. *Mol. Microbiol.* **78,** 947–963 (2010).
39. West, S. A., Griffin, A. S. & Gardner, A. Social semantics: altruism, cooperation, mutualism, strong reciprocity and group selection. *J. Evol. Biol.* **20,** 415-432 (2007).
40. Foster, K. R. & Bell, T. Competition, not cooperation, dominates interactions among culturable microbial species. *Curr. Biol.* **22,** 1845–1850 (2012).
41. Abrudan, M. I. *et al.* Socially mediated induction and suppression of antibiosis during bacterial coexistence. *Proc. Natl. Acad. Sci.* **112,** 11054–11059 (2015).
42. Rainey, P. B. & Rainey, K. Evolution of cooperation and conflict in experimental bacterial populations. *Nature* **425,** 72–74 (2003).
43. Scanlan, P. D. & Buckling, A. Co-evolution with lytic phage selects for the mucoid phenotype of *Pseudomonas fluorescens* SBW25. *ISME J.* **6,** 1148–1158 (2012).
44. Miskinyte, M. *et al.* The genetic basis of *Escherichia coli* pathoadaptation to macrophages. *PLoS Pathog.* **9,** e1003802 (2013).
45. Rainey, P. B. & Travisano, M. Adaptive radiation in a heterogeneous environment. *Nature* **394,** 69–72 (1998).
46. Konkol, M. A., Blair, K. M. & Kearns, D. B. Plasmid-encoded ComI inhibits competence in the ancestral 3610 strain of *Bacillus subtilis*. *J. Bacteriol.* **195,** 4085–4093 (2013).
47. Borkar, S. G. *Laboratory Techniques in Plant Bacteriology.*
48. Werb, M. *et al.* Surface topology affects wetting behavior of *Bacillus subtilis* biofilms. *NPJ Biofilms Microbiomes* **3,** 11 (2017).

FIGURE LEGENDS

Fig. 1 | Changes in pellicle productivity and morphology during evolution. (a) Biofilm productivities of six parallel Δ*eps*+Δ*tasA* co-cultures were systematically monitored (as CFU/ml) during ongoing evolution experiments. Productivities were assessed every 4th or 5th transfer. Relative frequencies of Δ*eps* and Δ*tasA* in the mixtures were assessed by plating the co-cultures onto media containing an appropriate antibiotic. Relative frequencies of the Δ*tasA* strain at each evolutionary time point (pulled from six parallel co-cultures) are shown as blue box plots. Boxes represent Q1–Q3, lines represent the median, and bars span from max to min (n=6). **(b)** Productivities of surface-colonizing Δ*eps* evolved in six parallel monocultures were systematically monitored as in (a). **(c)** Productivities of surface-colonizing Δ*tasA* evolved in six parallel monocultures were systematically monitored as in (a) and (b). **(d)** Pellicle morphology developed by the Δ*eps*+Δ*tasA* mix, and Δ*eps* and Δ*tasA* monocultures at the start and at the end of the evolution experiment. Pellicles were cultivated in 24 well plate (well diameter = 15 mm). Scale bar equals 10 mm. Morphology was tested in more than 10 independent experiments with similar results.

Fig. 2 | Complementation assay to recreate the evolved Δ*eps* phenotype. (a) Pellicle morphology developed by Δeps_{anc} (the ancestor Δ*eps* strain) and two isolates e4A and e6A that showed improved surface-colonizing properties and that were randomly selected from the evolved populations Δ*eps*4 and Δ*eps*6. Below, pellicle morphologies of Δ*eps*Δ*tasA*_$tasA_{anc}$ (Δ*eps*Δ*tasA* double mutant complemented with the native form of the *tasA* gene in the ectopic *amyE* locus) and Δ*eps*Δ*tasA*_$tasA_{Y124C}$ and Δ*eps*Δ*tasA*_$tasA_{G183C}$ (Δ*eps*Δ*tasA* double-mutants complemented with evolved forms of *tasA*). Pellicles were cultivated in a 24 well plate (well diameter = 15 mm). Scale bar equals 10 mm. Similar result was obtained in >5 independent experiments. **(b)** Productivities of surface-colonizing Δeps_{anc}, e4A, e6A, Δ*eps*Δ*tasA*_$tasA_{anc}$, Δ*eps*Δ*tasA*_$tasA_{Y124C}$ and Δ*eps*Δ*tasA*_$tasA_{G183C}$ were recorded as CFU/ml (n = 3 biologically independent samples). Asterisks indicate significant differences from Δeps_{anc} (*p < 0.05; **p < 0.01, ***p < 0.001; t-test, two-tail). **(c)**. Fitness of Δ*eps*Δ*tasA*_$tasA_{anc}$, Δ*eps*Δ*tasA*_$tasA_{Y124C}$, and Δ*eps*Δ*tasA*_$tasA_{G183C}$ when challenged with Δeps_{anc} in pellicle biofilm forming conditions (n = 4 biologically independent samples). Boxes represent Q1–Q3, lines represent the median, and bars span from max to min. Asterisks indicate statistically significant differences (**p < 0.01, ***p < 0.001; t-test, two-tail). For morphology (a), productivity (b) and fitness (c) studies, the complemented strains were grown in the presence of 0.2 mM IPTG to induce the expression of introduced *tasA* variants.

Fig. 3 | Fibre formation by native ΔSP-TasA and its cysteine-containing derivatives. **(a and d)** Transmission electron microscopy images of fibres formed by ΔSP-$TasA_{anc}$ (native TasA), **(b and e)** ΔSP-$TasA_{Y124C}$, and **(c and f)** ΔSP-$TasA_{G183C}$ on carbon-coated EM grids. For images a–c the scale bar equals 0.2 µm, for images d–f the scale bar equals 0.1 µm. Arrows indicate filaments of stiff parallel arrangement that were typically formed by cysteine-containing ΔSP-TasA variants. Expression, purification and EM analysis of the TasA variants were performed in parallel to ensure comparability. Similar results were obtained for 10 different micrographs obtained per each sample.

Fig. 4 | Investigation and recreation of the evolved Δ*tasA* phenotype. (a) Viscoelastic properties of pellicles developed by WT (wild-type *B. subtilis* strain NCBI 3610), e4A, and Mt1A (which is a Δ*tasA* isolate that shows improved surface-colonizing properties selected from the evolved population mix1), were compared. The storage modulus (G') and loss factors (G''/ G') of WT and e4A are similar, while Mt1A exhibits lower G' and loss factor, indicating more pronounced viscous properties of Mt1A pellicles as compared to those of WT and e4A. Boxes represent Q1–Q3, lines represent the median, and bars span from max to min (for WT n = 9; e4A n = 6; Mt1A n = 5 biologically independent samples). **(b)** Expression of *eps* gene in the Δ$tasA_{anc}$ (ancestor Δ*tasA*) strain and seven randomly selected evolved isolates that showed improved surface-colonizing properties was compared using corresponding strains carrying a P_{eps}-*gfp* reporter fusion (n = 8 biologically independent samples). Data points represent the mean and error bars represent standard error. **(c)** Pellicle morphology developed by two evolved Δ*tasA* isolates, t5A and Mt1A (Δ$tasA_{anc}$ and Δ*tasA*Δ*ptpZ*); below, zoom images of the surfaces of the t5A and Mt1a pellicles. Pellicle morphology of Δ$tasA_{hyEPS}$ (a Δ*tasA* strain with native *eps* promoter replaced with an IPTG-inducible promoter) grown without IPTG and Δ$tasA_{hyEPS}$ grown with 0.2 mM IPTG. Pellicles were cultivated in 24 well plate (well diameter = 15 mm). White scale bar equals 500 µm, black scale bar equals 10 mm. Similar result was obtained in 2 independent experiments **(d).** Productivities of surface-colonizing Δ$tasA_{anc}$, Δ$tasA_{hyEPS}$ (no IPTG), Δ$tasA_{hyEPS}$ (with 0.2 mM IPTG), t5A, Mt1A and Δ*tasA*Δ*ptpZ* were assessed as CFU/ml (n = 3 biologically independent samples). Boxes represent Q1–Q3, lines represent the median, and bars span from max to min. Asterisks indicate significant differences compared with Δ$tasA_{anc}$ (*p < 0.05; **p < 0.01, ***p < 0.001; t-test, two-tail).

Fig. 5 | Population structure and fitness of the evolved Δ*eps* and Δ*tasA* populations. (a) Four independently evolved Δ*eps* populations (Δ*eps*3, Δ*eps*4, Δ*eps*5, Δ*eps*6) were examined for diversity at the productivity level within the population. Specifically, 96 randomly selected isolates from each population were allowed to form pellicles that were then scored according to their performance: 0: ancestor-like residual pellicle to 3: strong pellicle (as for e4A or e6A). Each population is graphically

represented by a square made of 96 cubes. Colours of the cubes correspond to performance of the isolates: score = 0, white; 1, light grey; 2, dark grey; 3, black. **(b)** Changes in fitness in the Δ*eps*4 population thorough evolutionary time when challenged with Δeps_{anc} in pellicle biofilm forming conditions (n = 4 biologically independent samples). Data points represent the mean and error bars represent standard error. **(c)** Four independently evolved Δ*tasA* populations (Δ*tasA*3, Δ*tasA*4, Δ*tasA*5, Δ*tasA*6) were examined for diversity at the productivity level within the population, as described in (A). The results are represented graphically as described in (a). **(d)** Changes in fitness in the Δ*tasA*4 population thorough evolutionary time when challenged with $\Delta tasA_{anc}$ in pellicle biofilm forming conditions (n = 4 biologically independent samples). Data points represent the mean and error bars represent standard error.

Fig. 6 | Effects of Δ*eps* or Δ*tasA* evolutionary advantage on productivity of mixed pellicles. Productivities of pellicles formed by: Δeps_{anc}+$\Delta tasA_{anc}$, Δeps_{anc}+$\Delta tasA_{evolved}$, $\Delta eps_{evolved}$+$\Delta tasA_{anc}$, and $\Delta eps_{evolved}$+$\Delta tasA_{evolved}$ were compared. Six evolved Δ*eps* and Δ*tasA* isolates were incorporated into the analysis. Boxes represent Q1–Q3, lines represent the median, and bars span from max to min (for Δeps_{anc}+$\Delta tasA_{anc}$ co-culture n = 22; for e4C:t4B, e4C:t6B, e6A:t6B, e4A:t4B and e4A:t3C, n = 6; for e4C:t3C, e6A:t3C and e4A:t6B, n = 2; for other co-cultures n = 3 biologically independent samples). Asterisks indicate statistically significant differences from the ancestral mix (*$p < 0.05$; **$p < 0.01$, ***$p < 0.001$; t-test, two-tail).

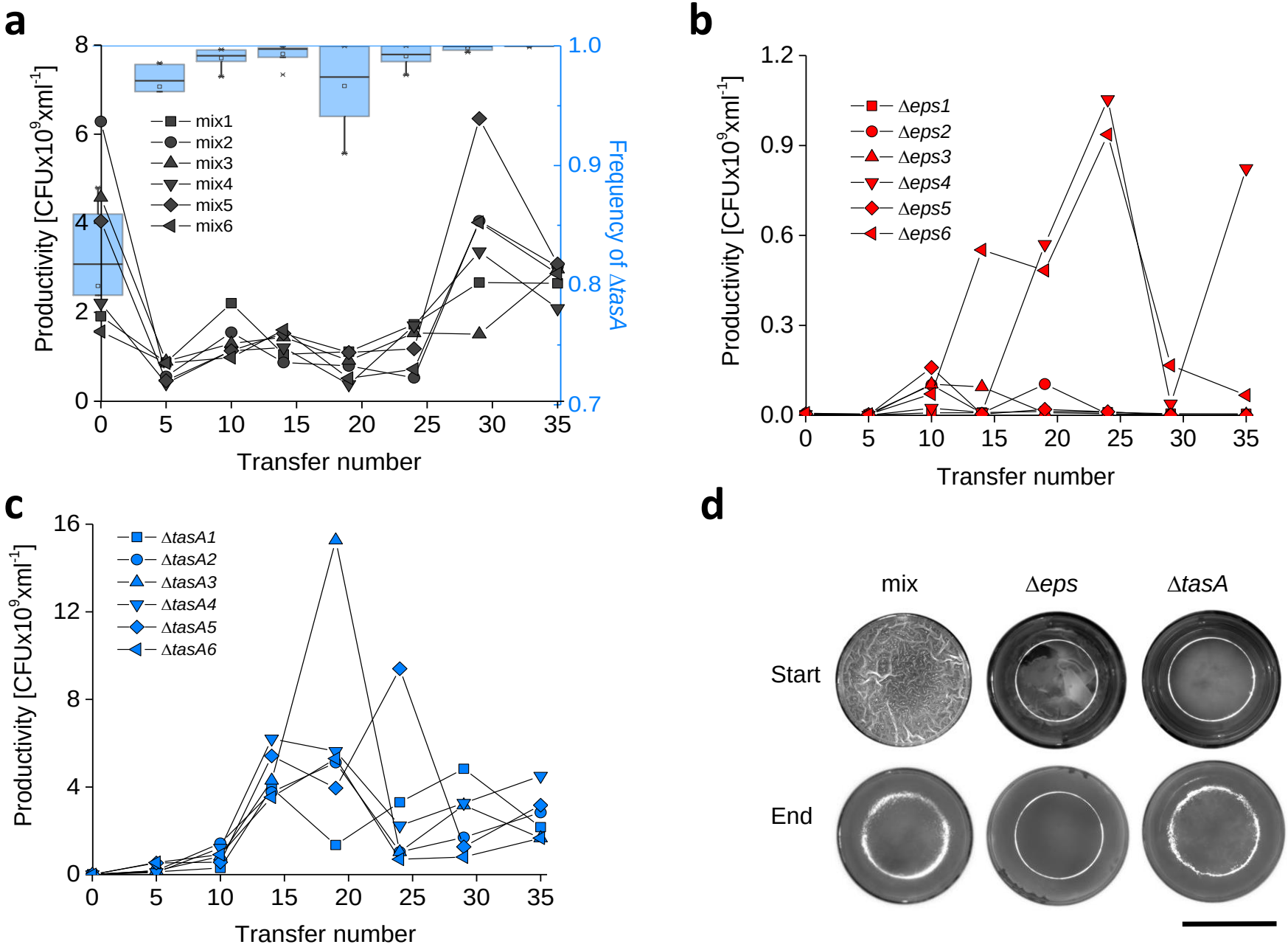
a
Productivity [CFUx10^9xml^-1]
Frequency of ΔtasA
Transfer number
mix1
mix2
mix3
mix4
mix5
mix6
b
Productivity [CFUx10^9xml^-1]
Transfer number
Δeps1
Δeps2
Δeps3
Δeps4
Δeps5
Δeps6
c
Productivity [CFUx10^9xml^-1]
Transfer number
ΔtasA1
ΔtasA2
ΔtasA3
ΔtasA4
ΔtasA5
ΔtasA6
d
mix
Δeps
ΔtasA
Start
End

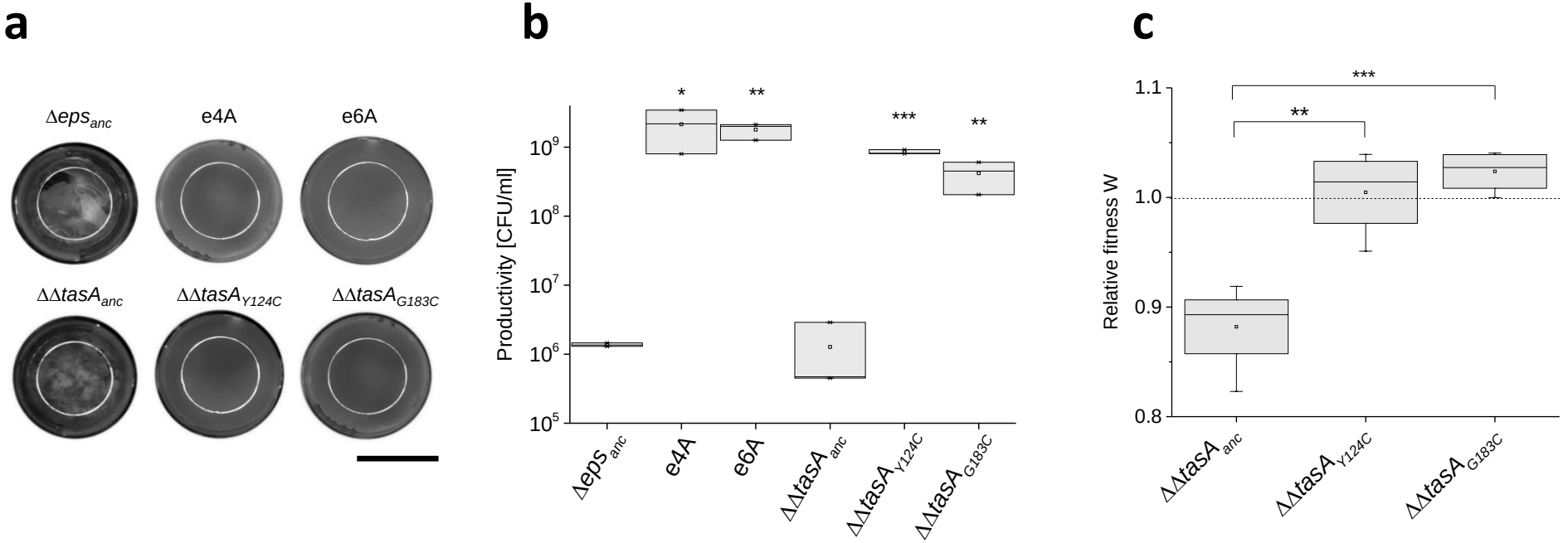
a
Δeps anc
e4A
e6A
ΔΔtasA anc
ΔΔtasA Y124C
ΔΔtasA G183C
b
Productivity [CFU/ml]
10^9
10^8
10^7
10^6
10^5
*
**
***
**
Δeps anc
e4A
e6A
ΔΔtasA anc
ΔΔtasA Y124C
ΔΔtasA G183C
c
Relative fitness W
1.1
1.0
0.9
0.8
***
**
ΔΔtasA anc
ΔΔtasA Y124C
ΔΔtasA G183C

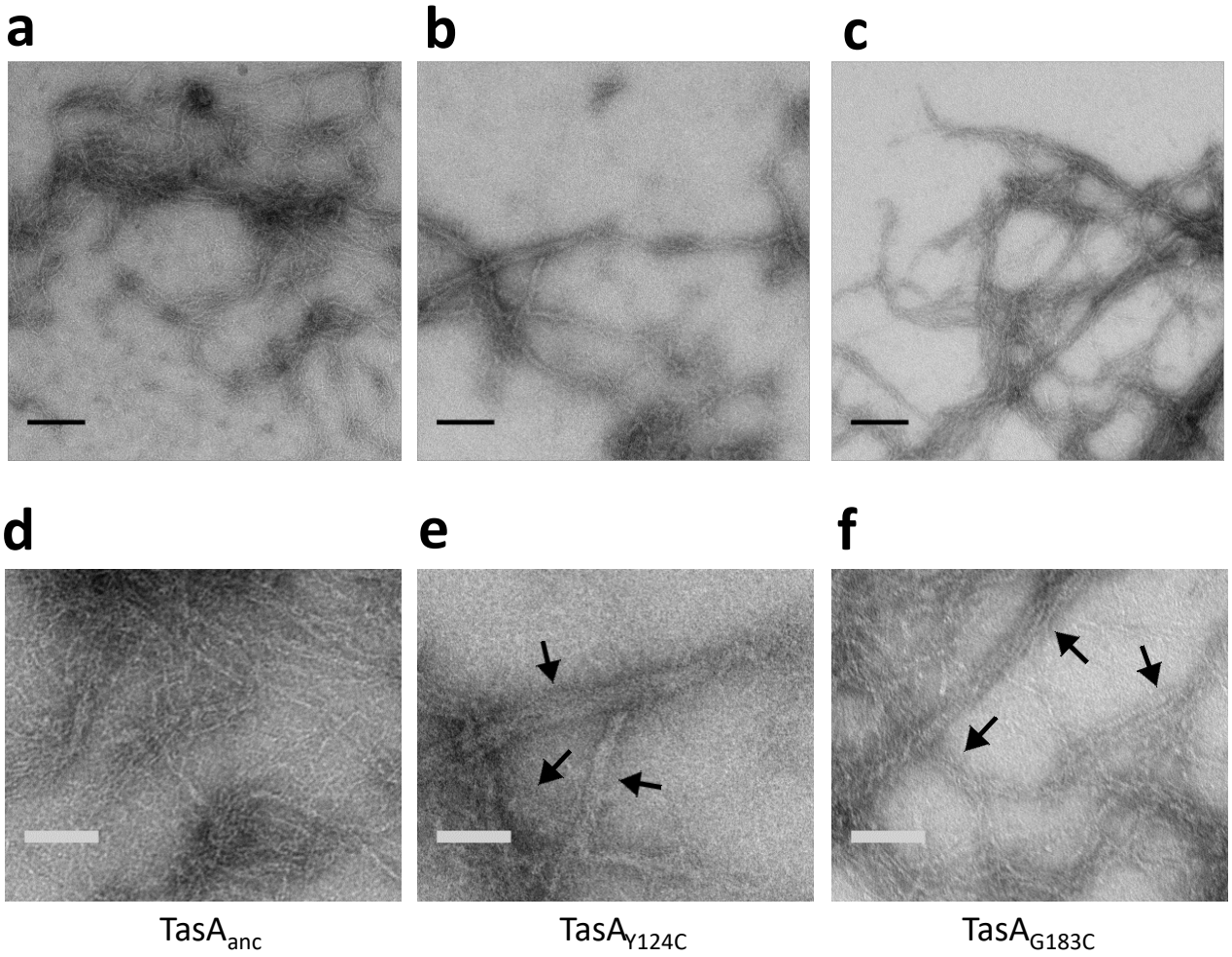
a
b
c
d
e
f
TasA$_{anc}$
TasA$_{Y124C}$
TasA$_{G183C}$

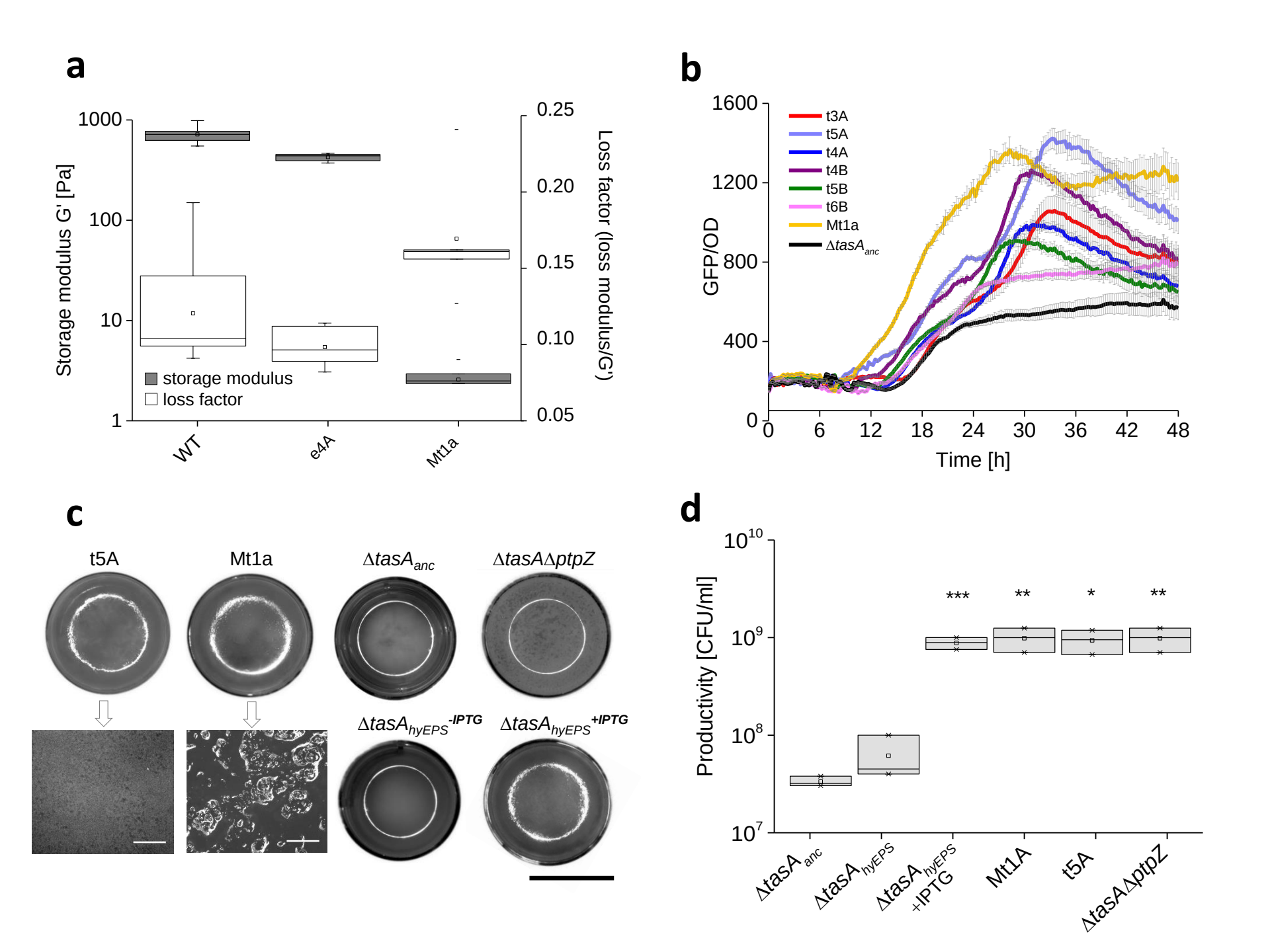
a
Storage modulus G' [Pa]
Loss factor (loss modulus/G')
storage modulus
loss factor
WT
e4A
Mt1a
b
GFP/OD
Time [h]
t3A
t5A
t4A
t4B
t5B
t6B
Mt1a
ΔtasA anc
c
t5A
Mt1a
ΔtasA anc
ΔtasAΔptpZ
ΔtasA hyEPS -IPTG
ΔtasA hyEPS +IPTG
d
Productivity [CFU/ml]
***
**
*
**
ΔtasA anc
ΔtasA hyEPS
ΔtasA hyEPS +IPTG
Mt1A
t5A
ΔtasAΔptpZ

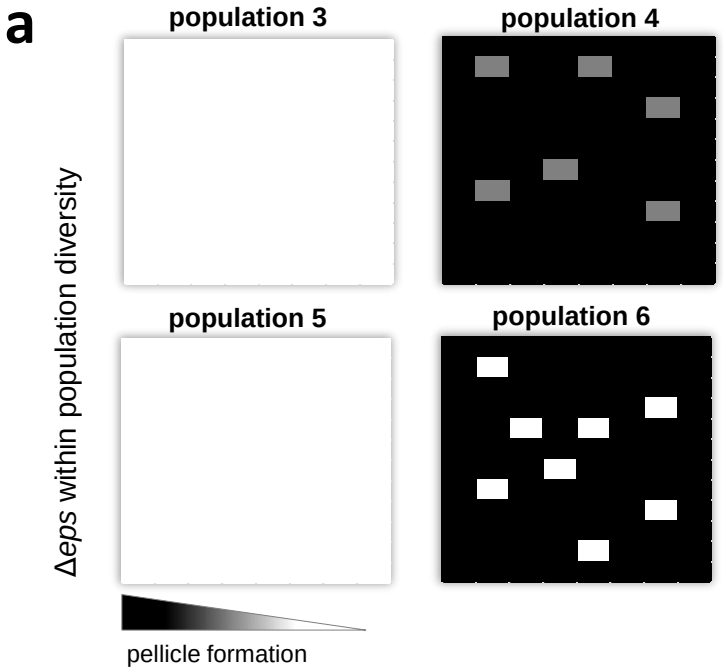
a
population 3
population 4
population 5
population 6
Δeps within population diversity
pellicle formation

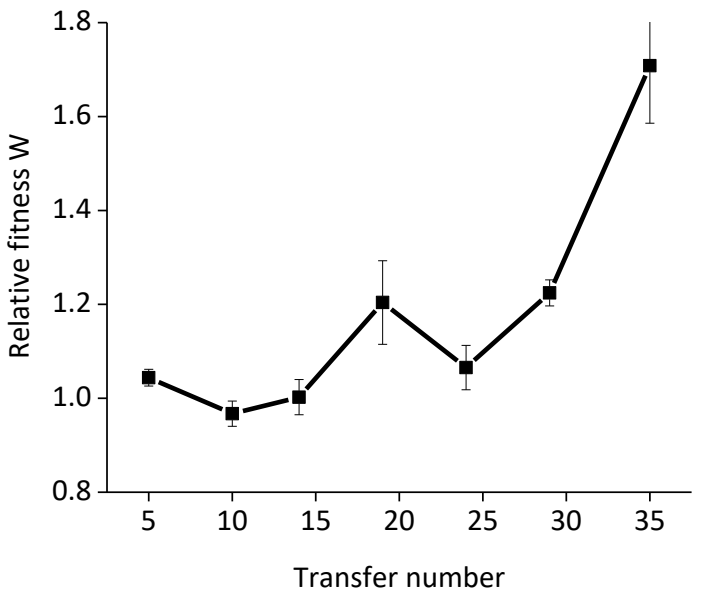
b
Relative fitness W
1.8
1.6
1.4
1.2
1.0
0.8
5
10
15
20
25
30
35
Transfer number

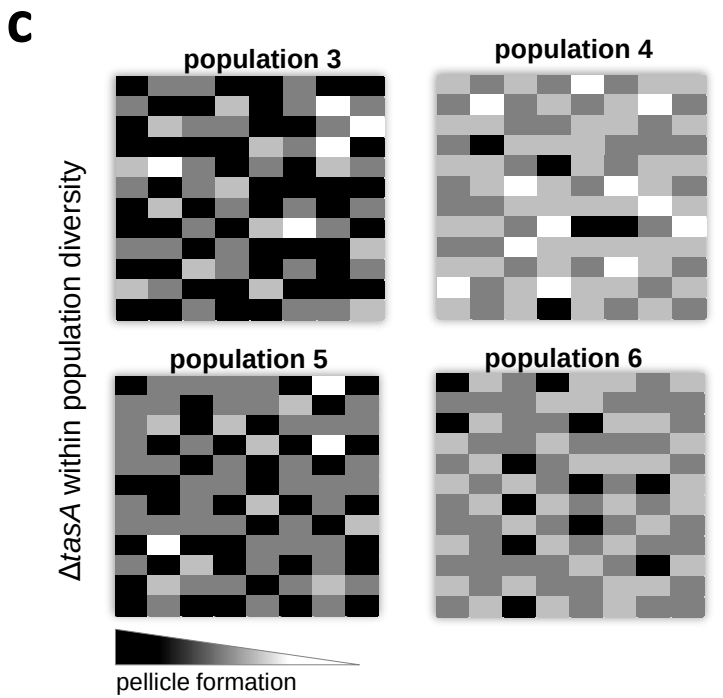
c
population 3
population 4
population 5
population 6
ΔtasA within population diversity
pellicle formation

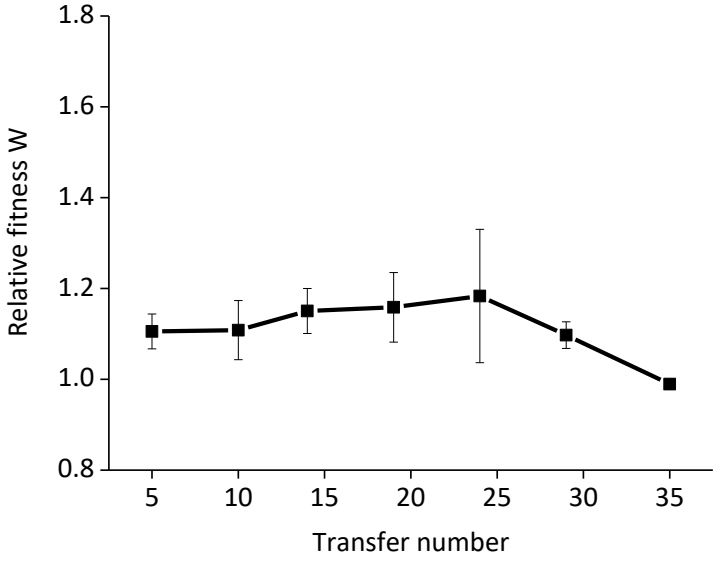
d
Relative fitness W
1.8
1.6
1.4
1.2
1.0
0.8
5
10
15
20
25
30
35
Transfer number

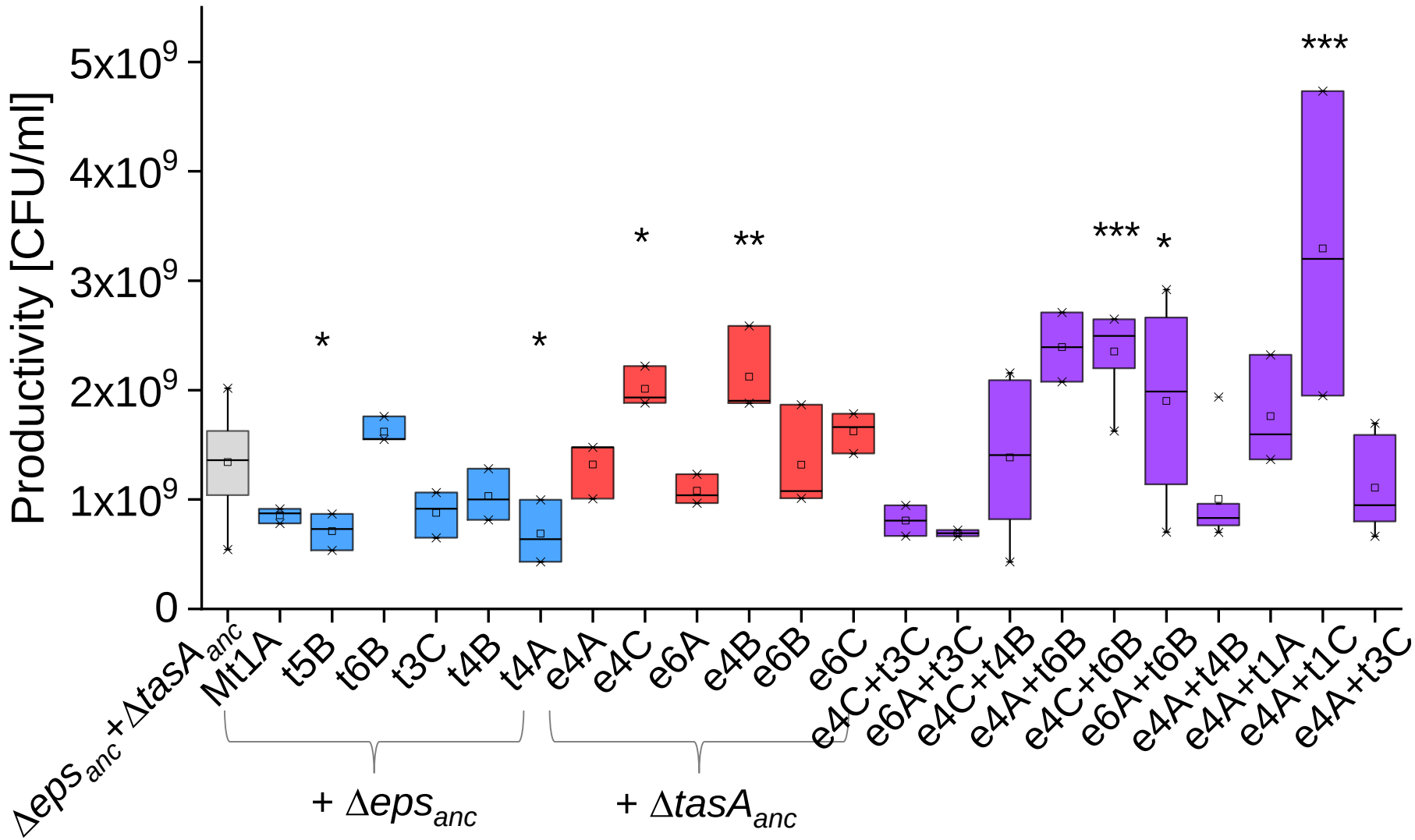
Productivity [CFU/ml]
5x10^9
4x10^9
3x10^9
2x10^9
1x10^9
0
*
*
*
**
***
*
***
Δeps_anc+ΔtasA_anc
Mt1A
t5B
t6B
t3C
t4B
t4A
e4A
e4C
e6A
e4B
e6B
e6C
e4C+t3C
e6A+t3C
e4C+t4B
e4A+t6B
e4C+t6B
e6A+t6B
e4A+t4B
e4A+t1A
e4A+t1C
e4A+t3C
+ Δeps_anc
+ ΔtasA_anc